ILSC ® 2013 Conference Proceedings

Validation of a computer model to predict laser induced thermal injury thresholds of the retina

Mathieu Jean and Karl Schulmeister

Reference information for this proceedings paper

Title: *Validation of a computer model to predict laser induced thermal injury thresholds of the retina*

Author: *Mathieu J, Schulmeister K*

Proceeding of the International Laser Safety Conference, March 18-21 2013, Orlando, Florida
Page 229-238

Published by the Laser Institute of America, 2013
Orlando, Florida, USA www.lia.org

VALIDATION OF A COMPUTER MODEL TO PREDICT LASER INDUCED THERMAL INJURY THRESHOLDS OF THE RETINA

Paper #1002

Mathieu Jean and Karl Schulmeister

Seibersdorf Laboratories;
Laser, LED and Lamp Safety Test House and Consulting, 2444 Seibersdorf, Austria

Abstract

We present a computer model for predicting the median dose (ED_{50}) that produces an ophthamoscopically detectable lesion in the retina. It consists of an optical model (beam propagation through the eye), a reflectance model (absorption distribution within the retinal tissues), a thermal model (solving the heat equation) and a damage model (based on the Arrhenius equation). The model was validated with 253 experimental ED_{50}s that cover the entire thermal regime in both macular and paramacular regions encompassing wavelengths between 413 nm and 1338 nm, pulse durations between 100 µs and 3000 s and retinal spot sizes ranging from minimum to 2 mm. These ED_{50}s are matched with a mean ratio of 0.93 and a standard deviation of 31 %. The largest ratio between model prediction and experimental data was 1.7. The applicability for using the model results for risk analysis for human exposure is discussed.

Introduction

Laser safety exposure limits are on an international level recommended by ICNIRP (International Commission on Non-Ionizing Radiation Protection, see e.g. [1]). The exposure limits are derived from experimental injury threshold data obtained from laboratory animal models. The most suitable model for human retinal damage is the non-human primate (NHP), especially the macaque family.

Over the past five decades, in-vivo studies have been undertaken for the purpose of determining the dose associated with 50% probability (ED_{50}) of producing an ophthalmoscopic visible lesion, which is commonly considered as threshold injury [2]. However, ethical and economical considerations restrain the available data. Additionally, the wide range of potential exposure conditions imply that in-vivo models solely cannot provide a complete data set for laser-induced retinal damage. We believe that computer modeling can be accurate enough in predicting threshold levels in order to: i) support setting exposure limits by interpolating experimental data and by evaluating complex exposure conditions, ii) give a-priori guidance for planning future experimental studies, iii) improve scientific understanding of laser-tissue interactions and iv) characterize if an exposure scenario for a specific product can lead to retinal injury or not, i.e. for risk analysis independent of MPEs.

Computer models for the prediction of retinal thermal injury are used since the 1970s and, as is our model, are all based on the same method: with the laser energy as source, the heat flow equation is solved, either analytically [3, 4] or numerically [5, 6], and thermal damage is calculated with the Arrhenius equation [5, 7]. Typically, models were compared to experimental ED_{50}s either for a specific parameter range in terms of wavelength and/or pulse duration (e.g. [3, 8]) or, for the cases of a wider parameter range, the discrepancy to experimental data was for instance of the order of 3 [5] i.e. not sufficient for providing the basis for setting safety limits.

Although our model uses the same basic method as previous models, it is, we believe for the first time, optimized in a systematic way and validated against all applicable experimental thermal injury threshold data that were identified in the literature. The 253 experimental data used for validation encompass most of the parameter range relevant to thermal damage, i.e. retinal spot size between minimum and 2 mm, pulse duration between 100 µs and 3000 s, wavelength between 413 and 1338 nm and pulse repetition rate between 0.0017 Hz and 9.1 Hz.

In the section “Model description”, we present the computer model set-up and the parameters. In the section “Model validation”, the agreement between model predictions and ED_{50}s is demonstrated. In the “Discussion”, we highlight the most critical model parameters, the range of applicability and we also describe the changes in the model for the prediction of the injury threshold for the human eye.

Model Description

Our computer model is split into five substructures. Laser beam propagation throughout the eye is modeled in a schematic eye for calculating the retinal spot size in accordance with the characteristics of the laser source. Ocular transmission accounting for wavelength and spot size dependence is based on in-vitro measurements and a scattering function. A reflectance model determines the distribution of light absorption within the retina, which is used as source term in the heat equation solved numerically by means of finite elements. Finally, the transient increase in temperature within the retina is used in a non-linear damage model derived from the Arrhenius equation in order to determine the injury level.

Most of the parameter values presented below result from a series of empirical adaptations (manual fitting) or partial optimization (systematic optimization of subgroups of parameters) for the purpose of finding the best settings in accordance with the investigated data. A trade-off between "physics and parameter adjustment" is thought to be practically unavoidable in order for our model to be applicable over the entire thermal regime given the fact that many properties are known only inaccurately (e.g. parameters of the damage model) or subject to large biological variability (e.g. pigmentation, optical quality). This is even beneficial since the proposed model is optimized for matching exclusively experimental results obtained under specific conditions (i.e. in laboratory).

The figures of merit that were used to systematically optimize the model parameters were the overall standard deviation of ratio R_{ED50} (model threshold to ED_{50} ratio) as well as the significance of linear regression (p-value) against wavelength, pulse duration and retinal spot size. If a correlation of R_{ED50} with any of these parameters is found, then this indicates that the model can be further improved until ideally no correlation ($p \rightarrow 0$) is found. The goal of the optimization was to minimize both standard deviation and correlation.

1. Optics of the eye

We use an optical model accounting for the dependence on wavelength and corneal diameter in order to obtain a more accurate estimation of the retinal spot size than provided by the thin lens equation. A four-surface schematic eye with homogenous media is derived from the Le Grand full theoretical model for the relaxed human eye [9] for the young Rhesus monkey by scaling all elements by a factor 0.8 (for instance, 0.71 has been used in [10]). This scaling factor gives a nominal focal length of 13.35 mm at 590 nm which is corroborated within ±0.7 mm by several studies [11, 12, 13]. The schematic eye of the Rhesus monkey can be downscaled from the human one [14]. The wavelength-dependent refractive indices are computed in the form of the Herzberger's dispersion formula (for numerical values, see [15]). All aberrations but longitudinal chromatic aberration are disregarded.

Given the far-field divergence, wavelength of radiation and beam size at the corneal plane of the light source, the retinal image size is calculated by ray-tracing using the ray transfer matrix analysis for Gaussian beams [16, 17] under the assumption of axial symmetry. For the purpose of fitting ED_{50}s, the assumption of a minimum spot size turned out to be necessary (as in [18]). An optimum value of 65 µm is used here, close to the 57/64 µm [19] and 70 µm [7] used in earlier models. At 590 nm, the nominal focal length being 13.35 mm, it corresponds to a minimum source size of 4.87 mrad, which is used for computing the minimum spot size at all wavelengths. Due to chromatic aberration, we obtain for instance 78 µm and 97 µm at 440 nm and 1060 nm respectively (for a beam diameter of 3 mm at the cornea).

2. Ocular transmission

Light attenuation by the anterior ocular media is based on ex-vivo measurements [20], where the so-called total transmission T_{total} is used as an upper bound (large irradiance profiles) while the direct transmission is assumed to provide a measure for collimated beams. The ratio between these two measures can be fitted by the function $g(\lambda)$ where λ is the wavelength of radiation (see Equation. 1).

$$\begin{cases} T_{eff}(\lambda, \vartheta) = T_{total}(\lambda) . [\, 1 - g(\lambda) . h(\vartheta)] \\ g(\lambda) = e^{-0.0012 . \lambda} \\ h(\vartheta) = 0.5\, e^{-\vartheta/600} \end{cases}$$

Equation. 1. Spot size (ϑ in µm) and wavelength (λ in nm) dependent effective transmission (T_{eff}) based on transmission data (T_{total})

This mathematical approximation allows for modulating the effective ocular transmission T_{eff} as a function of spot size. For this purpose, the function $g(\lambda)$ is weighted by a spot-size dependent function, intended to represent the amount of light actually focused in the spot, the rest being scattered out. It is chosen arbitrarily as the cumulated fraction of the Heyney-Greenstein phase function (see [21]), given an anisotropy factor of 0.94 and a scattering center located at the second nodal point (approximated by the function $h(\vartheta)$, ϑ being the spot size). This empirical approach is thought to be consistent with the forward-scattering characteristics of the eye where intra-ocular

scattering is the main factor for lateral losses [22, 23], presumably impacting small spots to a larger extent than large ones.

3. Optics of the retina

Within the retina, three absorbers are considered, namely: macular carotenoids (also known as macular or yellow pigment), melanin and hemoglobin. Macular pigments are concentrated in the neural retina around the Henle's fiber layer [24, 25]. Melanin is, in the form of melanosomes, almost restricted to the apical part of the retinal pigment epithelium (RPE) cells in young subjects [26] while it is to be found as melanosomes (particles) and melanocytes (cells forming melanin) in the choroid (CHO) [27]. In this layer, large vessels in the outer choroid and capillaries in the inner choroid compose most of the retinal vascular system [28]. Choroidal blood is assumed to be exclusively oxi-hemoglobin. Bulk absorption by water within the retina is neglected. Attenuation within the sclera is also neglected since it is tremendously lower than in the RPE or CHO [29, 30]. All pigments are assumed to be homogeneously distributed in their respective layers and the Beer-Lambert's law is applied to describe attenuation. Homogeneity of pigmentation within the RPE is a reasonable assumption since the pulse durations regime that we are concerned with (>50 µs) exceeds greatly thermal relaxation of melanin granules [3, 31] and even exceed the diffusion time between granules, whose characteristic spacing is in the order of 1-2 µm [4].

Within the retina, light is also subject to reflection and back-scattering. Two major sites of reflection are located in front of the RPE and at the interface between CHO and sclera, as in the model II of fundus reflectance proposed by Delori and Pflibsen [28]. Reflection is considered as being specular in order to simplify the distribution of absorption within the retinal layers. Multiple reflections are neglected. The wavelength-dependent function of scleral reflection we propose is a fitting of experimental data [29].

The different sensitivity of macular and paramacular regions to laser light [e.g. 32, 33, 34] is accounted for by two retinal models. RPE optical density, which is larger in the macula [35] because RPE cells are thicker [36], narrower [37] and more densely pigmented [38, 39], is expected to explain most of the difference. In both models, the choroid is identical although thickness [40, 36] and pigmentation [36] actually vary with eccentricity.

Between the pigmented RPE and CHO is a thin non-pigmented intermediate layer, anatomically representing the basal part of RPE cells and the Bruch's membrane [36]. The thickness of these three layers was optimized. Noticeably, the 6 µm thick RPE and 4 µm thick pigment-free layer combination has been used in an earlier model [41].

Table. 1. Geometric and optical properties of the retina (λ: wavelength in nm)

Layer	Thickness [µm]	Pigmentation [%]	Reflection at front [%]
Pre-retinal tissues	∞	-	-
Henle's fiber (macula only)	7	100 (MP)	-
Photoreceptors	60	-	-
pigmented RPE (macula)	10	100 (ME)	2.1
pigmented RPE (paramacula)	6	100 (ME)	1.7
non-pigmented RPE	4	-	-
Choroid	170	11.4 (ME) / 30 (BL)	-
Sclera	∞	-	$1 - 0.67\, e^{-3\,10^{-6}.(\lambda-660)^2}$

Pigment	Absorption coefficient [cm^{-1}]
Macular pigment (MP)	ref. [42]
Melanin (ME)	$3.85\ 10^{14}\ .\ \lambda^{-4.2}$
Oxi-hemoglobin (BL)	ref. [44]

Pigment concentrations have been optimized while spectra of absorption are fittings of values found in the literature (macular pigment [42], melanin [43] and blood [44]). Absorption by melanin was optimized. Model parameters are summarized in Table. 1. The absorption of total intra-ocular energy is distributed as shown in Figure. 1.

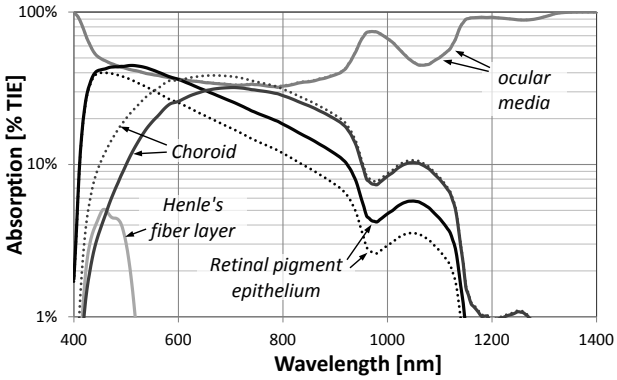

Figure. 1. Absorption of total intraocular energy (TIE) throughout the eye for a collimated beam in the macula (solid lines) and paramacula (broken lines)

4. Retinal temperature distribution

The heat conduction equation is solved numerically by means of finite elements using a commercial package (Comsol 3.5a, Comsol AB, Stockholm, Sweden, 2008) under the assumption of axial symmetry. Thermal properties are homogenous and set equal to those of water, since the water content of the retina exceeds 80% [45] and the volumetric heat capacity of melanosomes is similar to that of water within 10% [4, 46]. Thermal properties are considered temperature-independent. Consequently, temperature rise is linear with respect to power. Initial temperature is set to 37°C. The energy absorbed within the ocular media is neglected in the thermal model.

5. Damage evaluation

Thermal damage is based on the concept of accumulation of microscopic sublethal damage [47] which ultimately leads to cell death by apoptosis or necrosis [48]. The additivity of sublethal damage is particularly striking for multiple pulses [49]. The so-called Arrhenius model based on the eponymous equation describes the temperature-dependent rate of reaction and gives a measure of local damage when integrated over time (Equation. 2). The integral value (Ω) of 1 is commonly accepted as a threshold for cellular irreversible transition. The values of A and E used here are comparable in magnitude to those found in the literature (see [50]).

$$\begin{cases} rate: \ k(t) = A\, e^{-E/T(t)} \\ damage: \ \Omega = \int_0^{\tau} k(t)dt \end{cases}$$

Equation. 2. First-order Arrhenius model

Table. 2. Thermal properties of the retina and constants of the damage model

	Value	*Unit*
Thermal model		
conductivity	0.6305	$W.(m.K)^{-1}$
specific heat	4178	$J.(kg.K)^{-1}$
density	992	$kg.m^{-3}$
initial temperature	310.5	K
Damage model		
Lesion diameter (MVL)	50	µm
pre-exponential factor (A)	1.05×10^{95}	s^{-1}
inactivation energy (E)	72000	K

As shown histologically, threshold lesions are mostly confined to the RPE [11, 51]. The damage model is thus applied to this layer only, where the increase in temperature is also the highest. A constant MVL diameter of 50 µm is found to be optimal in this model for non-human primates even for the case of collimated beams (see discussion). Parameters of the thermal and damage models are tabulated in Table. 2.

Model validation

6. Experimental data

The computer model is intended to simulate the experimentally determined median dose inducing an ophthalmoscopic minimum visible lesion (MVL) assessed within two days in anesthetized Rhesus monkey subjects. Damage mechanisms other than thermal are not discussed. For the sake of consistency, several restrictions apply to the selection of studies to be modeled in the process of validation of the model.

The standard assessment of lesions is performed with an ophthalmoscope or fundus camera since other detection techniques – including the invasive or cognitive ones – have different sensitivities (see e.g. [10, 52]). Lesion assessment delay is restricted to 10 minutes until 48 hours after exposure. Within this delay, thermally-induced thresholds tend to decrease [e.g. 32, 53] but remain within eye-to-eye variability [54] or in some cases do not vary at all between 1h and 24h (e.g. [55]). Among 32 ED_{50}s given at both 1h (or less) and 24/48h [53, 54, 56, 57, 58, 59], the 1h to 24h ratio is 1.12 ±0.17. Consequently, we chose to pool them together. Thresholds reported as lowest ophthalmoscopically visible lesions are inconsistent with ED_{50}s since the average ratio is approximately 1.7 between these two measures (see [33, 60, 61]).

Any strong alteration of the optics of the normal eye (e.g. no correction for refractive error larger than 0.5 D, aphakic eye or wavefront correction) is inconsistent with the optimization of the properties of the normal relaxed naked eye. If paramacular ED_{50}s are given at different eccentricities for the same exposure condition, we select only the lowest of all (e.g. at 15° temporal in [55]). Since inter-species differences have been pointed out between Rhesus monkey (macaca mulatta) and Cynomolgus monkey (macaca fascicularis) regarding eye size [13, 14], optical quality [12, 62], central retinal morphology [63] and sensitivity to laser light (compare e.g. Lund D. et al. [57] and Lund B. et al. [64]), ED_{50}s obtained with Cynomolgus monkeys are not considered in this work.

Regarding the laser emission itself, it is unclear whether the damage mechanism can be strictly thermal

for pulses slightly shorter than 100 µs or not. Therefore, pulse durations shorter than 100 µs are not considered here, including mode-locked and Q-switch emissions. Photochemical mechanisms are avoided by selecting only 1h ED_{50}s at wavelengths below 580 nm when the exposure duration exceeds 10 s [53, 54].

Following these criteria, 43 threshold data have been excluded (from 10 studies): [10, 19, 57, 64, 65, 66, 67, 68, 69, 70] and 253 threshold data published in 31 studies are found applicable to model validation: [10, 11, 18, 19, 32, 33, 53, 54, 56, 57, 58, 59, 60, 61, 70, 71, 72, 73, 74, 55, 75, 76, 77, 78, 79, 80, 81, 82, 83, 84, 85].

Due to patent inconsistencies discussed in Lund et al. [53], data below 580 nm from Ham et al. [70] are excluded (4 data; exposure characteristics: 1 s, large spot, blue/green wavelengths, 48h). These thresholds show a wavelength-dependent trend typical of photochemical damage, i.e. thresholds are suspiciously low for 1-s exposures. Lund et al. [53] thus produced new data which are significantly higher and consistent with a purely thermal interaction. A second set of data from Lund et al. [57] (8 data; exposure characteristics: 0.1 s, large spots, 515 nm) is also excluded since a more recent study in which these exposures have been repeated [58] and support that the previous ED_{50}s were abnormally low. Additionally, two ED_{50}s at 1315 nm (300 µs [68]) are inconsistent with our model (predicted thresholds are 7 to 10 times lower than the ED_{50}s). Since data from Lund et al. [77] (1318-1338 nm, 650 µs) can be fitted by our model with a discrepancy of only 13%, we decided not to include the first set of data in our model validation. A possible explanation for the inconsistency of the experimental data is that in the NIR range between 1300 nm and 1400 nm, ocular transmission and retinal absorption are extremely low (less than 11% and 1% of total intraocular energy, respectively). Given inter-subject variability, a relative high variability in thresholds is expected and might explain why the data by Zuclich et al. are unexpectedly high.

7. Model thresholds against ED50s

Using the proposed model, 253 experimental ED_{50}s are simulated following the specifications provided by the authors of the respective study. Each damage threshold obtained with our model is compared with its experimental counterpart in terms of total intraocular energy (R_{ED50}: model to ED_{50} ratio). Overall results are tabulated in Table. 3. According to the Shapiro-Wilk test, the set of data is significantly drawn from a normally distributed population ($p < 0.001$). Remarkably, all samples lie within ± 2.3 SD and 65% are within ± 1 SD. A histogram of ratios and the corresponding normal model are shown in Figure. 2.

In Figure. 3, scatter plots depict the dispersion of individual ratios as a function of retinal spot size (nominal published values), pulse duration and wavelength of radiation. It is of importance to notice that dispersion is relatively constant over these variables, overall as well as when retinal sites are considered separately.

Table. 3. Most relevant estimators of overall success; normality is tested over 12 non-overlapping discrete intervals of constant size on a log scale

	Value
samples	253
Estimators	
mean ratio	0.93
standard deviation (SD)	0.31
lowest ratio	0.51
highest ratio	1.72
ratios within 1 SD*	165
Gauss model	
coefficient of determination (r^2)	0.93

**) i.e. between 0.71 and 1.22*

The mean of R_{ED50} and SD for the two groups are 0.93 /0.24 (macula, 75 samples), and 0.93/0.33 (paramacula, 178 samples). At the 0.01 level, means are not significantly different from each other but variances are. Regarding the delay of lesion assessment after exposure, mean and variance are not significantly different at the 0.01 level between ≤1h ED_{50}s and 24/48h ED_{50}s.

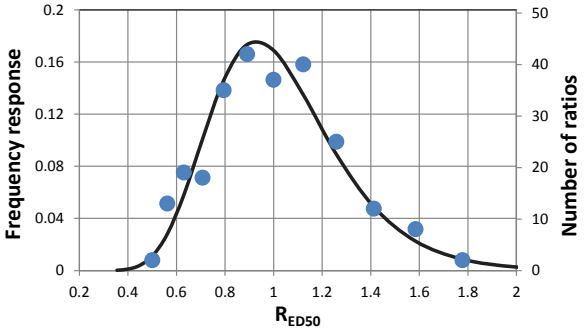

Figure. 2. Frequency response as a function of R_{ED50} (full circles, grouped into bins of constant size on log scale, both axes) and the corresponding normal distribution (line, left axis)

Discussion

The modeling of macular and paramacular exposures, which can be achieved by varying the thickness of the RPE solely and additionally adding macular pigment, is a feature (not implemented in other models) allowing us to cover the thermal regime extensively (72% of our ED_{50} set involves paramacular exposures). Although other possibilities have been considered, varying the RPE melanin concentration yields slightly poorer results for short paramacular exposures. The modeling of paramacular exposures is limited by our optical model, in which eccentricity is not accounted for. A refined optical model applied to laser-induced retinal damage has been proposed in [86]. Nevertheless, the optical quality of the human eye does not to vary to a large extent up to 20° eccentricity [87] and threshold damage shows no more than 25% variation in up to 50° in the Rhesus monkey [55].

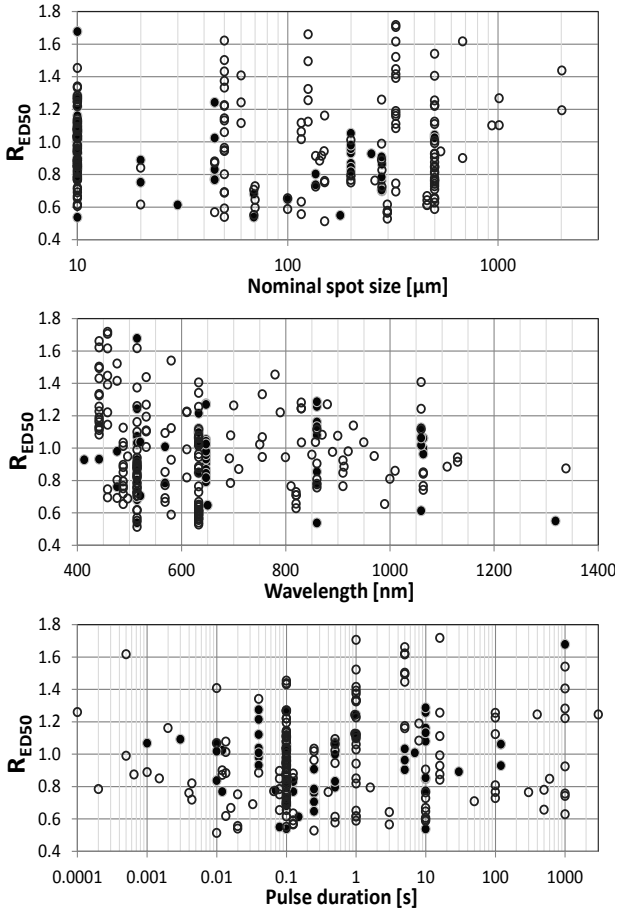

Figure. 3. Distribution of all 253 R_{ED50} against retinal spot size (if not explicitly mentioned by the authors, a sample is arbitrarily plotted at 10 µm for the sake of legibility), pulse duration and wavelength; macular (full circles) and paramacular exposures (open circles)

8. Minimum spot size behavior

We found that ED_{50}s obtained with nearly collimated beams are best fitted by assuming a minimum spot size of 65 µm at best focus in the normal relaxed eye. Although smaller spots at the retina close to the diffraction-limited image can be actually achieved after adjustment [22, 88], the observed average minimum spot size (MSS) is rather in the order of 30 µm to 80 µm [10, 51, 89]. This can be due to several factors: i) uncontrolled inter-subject variability and small refraction errors, for instance a 0.25 D error can increase the spot size from 20 µm to 50 µm [2, 64], ii) the retinal spot size is thought not to be constant for all exposure durations due to residual movements even in anesthetized subjects [11, 88, 90], iii) the size of the source term in the heat equation can be larger than the observed or "theoretical" spot size [91] for instance due to intra-retinal scattering [92]. In earlier models, values ranging between 35 µm and 70 µm for exposures in the visible spectrum have provided good agreement with ED_{50}s [5, 7, 19]. As used in our model, a MVL diameter of 50 µm is consistent with ophthamoscopically detected lesions confirmed by histopathological sections to range from 40 µm to 80 µm [52, 71, 91]. This minimum spot size effect is also seen experimentally and discussed in [92].

9. Transitions to other damage mechanisms

For exposures shorter than 100 µs, the model predicts higher thresholds than experimental ED_{50}s. Nonlinear damage mechanisms such as micro-cavitation prevail for laser pulse durations shorter than 5-50 µs [93]. Between 5 µs and 100 µs, it is still unclear if purely linear thermal mechanisms are suitable for explaining the threshold trend. The modeling of localized absorption in the melanosomes could provide a better approach in this transition domain [4]. The modeling of hot spots (spikes in the beam profile) is also necessary for an accurate modeling of the temperature rise in the microsecond range.

Regarding very long exposures (> 10 s, 33 samples), 6 1h-ED_{50}s are obtained for emissions where photochemical damage is observed 24h after exposure, further supporting the observation that lesions observed at 1h are thermal in nature. These results also suggest that it is not essential to take blood perfusion or residual eye movements into account. From a physics standpoint, these two phenomena have an effect on the decrease in temperature for a given retinal exposure level [94] and on the threshold level [95]. We could however fit long exposures well without including these components. Either the components actually have little effect on the threshold or our choice

of Arrhenius parameters has a compensation effect for very long exposures where threshold temperature is relatively low (approximately 9 K above body temperature after 1000 s). Noticeably, the first-order Arrhenius model seems to be applicable to thermal injury at temperatures as low as 6 K [96].

10. Application to humans

The ultimate aim of the experiments on laboratory animals and the model proposed herein is to set appropriate exposure limits for humans as well as to provide a basis for injury level analysis. Thermally-induced MVLs obtained in human subjects are systematically and significantly higher than in the Rhesus monkey both in macula and paramacula [Stuck84, Ham89], mostly attributable to a lighter pigmentation of the human retina [98, 99]. Nevertheless, histological investigations show that suprathreshold foveal lesions might be more severe in humans at identical power (100 mW, 488 nm, 50 ms [100]) and we cannot rule out the fact that accidental exposures in awake humans might occur with a retinal spot size smaller than the MSS used in our model, may it be only in the fovea where reduced intra-retinal scattering has to be assumed [Schulmeister06].

For these reasons, to model the injury level of humans, we propose to use a MVL diameter of 20 μm and a MSS of 25 μm (i.e. 1.5 mrad, as set in safety guidelines), instead of 50 μm and 65 μm respectively for the Rhesus monkey (this uncertainty in minimal spot size is also the reason why a reduction factor of 10 or larger is needed for the exposure limits for the minimal image case). This modification systematically lowers model thresholds, being mostly effective for short exposures and collimated beams. Such a model should provide conservative ED50 values even for foveal exposures in highly pigmented individuals with perfect visual acuity. Besides the uncertainty range of 1.7, an additional factor can be used to obtain a level which can be characterized as “negligible risk for injury”. It is noteworthy to mention that a factor of 2 relative to the ED_{50} corresponds to a probability of damage of 0.4% ($ED_{0.4}$) if we assume a slope (ED_{84}/ED_{50}) of 1.3 in probit analysis, which can be regarded as reasonably conservative.

Conclusion

The computer model proposed in this study has been optimized for the purpose of fitting thermally-induced retinal damage (median dose or ED_{50}) in the Rhesus retina, which is achieved against a set of 253 experimental data with a standard deviation of only 31%. This model is the first to be validated for both macular and paramacular exposures and for the full range of applicable wavelengths, retinal spot sizes and exposure durations – with the exception of pulse durations shorter than 100 μs. The validation shows that lesion thresholds can be predicted with relatively small uncertainty ranges for exposures at which no experimental data is available yet, including multiple irregular pulses, complex beam profiles and scanning. For the application of the model to the human eye, we propose slight modifications regarding retinal spot size and diameter of threshold lesion.

References

[1] International Commission on Non-Ionizing Radiation Protection (1996) Guidelines on limits for laser radiation of wavelengths between 180 nm and 1,000 μm, Health Phys 71:5.

[2] Sliney D.H., Mellerio J., Gabel V.-P. and Schulmeister K. (2002) What is the meaning of threshold in laser injury experiments? Health Phys 82:3.

[3] Birngruber R., Hillenkamp F. and Gabel V.-P. (1985) Theoretical investigations of laser thermal retinal injury, Health Physics 48:6.

[4] Thompson C.R., Gerstman B.S., Jacques S.L. and Rogers M.E. (1996) Melanin granule model for laser-induced thermal damage in the retina, Bull Math Biol 58:3.

[5] Takata A.N., Kuan L.P., Goldfinch L. et al, (1974) Thermal model of laser-induced eye damage, USAF School of Aerospace Medicine, Final report. Brooks, Texas.

[6] Glenn T.N., Rastegar S. and Jacques S.L. (1996) Finite element analysis of temperature controlled coagulation in laser irradiated tissue, IEEE Trans Biomed Eng 43:1.

[7] Welch A.J. and Polhamus G.D. (1984) Measurement and prediction of thermal injury in the retina of the Rhesus monkey, IEEE Trans Biomed Eng vol. 31:10.

[8] Polhamus G., Zuclich J., Cain C. et al. (2003) Model predictions of ocular injury from 1315 nm laser light, Ed. Stuck B.E. et al., Proc. of SPIE vol. 4953, 91-100.

[9] Atchison D.A. and Smith G. (2000) Optics of the human eye, Butterworth-Heinemann, ISBN 0750637757.

[10] Birngruber R., Gabel V.-P. and Hillenkamp F. (1983) Experimental studies of laser thermal retinal injury, Health Phys 44:5.

[11] Ham W.T., Geeraets W.J., Müller H.A. et al. (1970) Retinal burn thresholds for the Helium-Neon laser in the Rhesus monkey, Arch Ophthal 84.

[12] Medeiros J.A., Borwein B. and McGowan J.W. (1979) Application of optical transform techniques for laser irradiation of retina, Invest Ophthal Vis Sci 18:6.

[13] Lapuerta P. and Schein S.J. (1995) A four-surface schematic eye of macaque monkey obtained by an optical method, Vis Res 35:16.

[14] Qiao-Grider Y., Hung L.-F., Lee S.-C. et al. (2007) Normal ocular development in young rhesus monkeys, Vis Res 47:11.

[15] Navarro R., Santamaria J. and Bescos J. (1985) Accommodation-dependent model of the human eye with aspherics, J Opt Soc Am 2:8.

[16] Gerrard A. and Burch J.M. (1975) Introduction to matrix methods in optics, Dover Publications, ISBN 0486680444.

[17] Rockwell B.A., Hammer D., Kennedy P. et al. (1997) Retinal spot size with wavelength, Ed. Jacques S.L., Proc. of SPIE vol. 2975.

[18] Lund D.J., Edsall P. and Stuck B.E. (2008) Spectral dependence of retinal thermal injury, J Laser Appl 20:2.

[19] Connolly J.S., Hemstreet H.W. and Egbert D.E. (1978) Ocular hazards of picosecond and repetitive-pulsed lasers Volume II, USAF School of Aerospace Medicine, Report SAM-TR-78-21, Brooks, TX.

[20] International Commission on Illumination (2012) A computerized approach to transmission and absorption characteristics of the human eye, Report CIE 203:2012.

[21] Binzoni T., Leung T.S., Gandjbakhche A.H. et al. (2006) The use of the Henyey-Greenstein phase function in Monte Carlo simulations in biomedical optics, Phys Med Biol 51:17.

[22] Birngruber R., Drechsel E., Hillenkamp F. & Gabel V.P. (1979) Minimal spot size on the retina formed by the optical system of the eye, Int Ophthal 1:3.

[23] Pinero D.P., Ortiz D. and Alio J.L. (2010) Ocular scattering, Optom & Vis Sci 87:9.

[24] Subczynski W.K., Wisniewska A. and Widomska J. (2010) Location of macular xanthophylls in the most vulnerable regions of photoreceptor outer-segment membranes, Arch Biochem Biophys 504.

[25] Borland R.G., Smith P.A. and Owen G.P. (1992) A model for the prediction of eye damage from pulsed lasers, Laser light Ophthal 5:2.

[26] Delori F.C., Goger D.G. and Dorey C.K. (2001) Age-related accumulation and spatial distribution of lipofuscin in RPE of normal subjects, Invest Ophthal & Vis Sci 42:8.

[27] Beatrice E.S. and Shawaluk P.D. (1973) Q-switched Neodymium laser retinal damage in Rhesus monkey, Memorandum M73-9-1, Department of the Army, Frankford Arsenal, Philadelphia.

[28] Delori F.C. and Pflibsen K.P. (1989) Spectral reflectance of the human ocular fundus, Appl Opt 28:6.

[29] Vogel A., Dlugos C., Nuffer R. and Birngruber R. (1991) Optical properties of human sclera and their consequences for transscleral laser applications, Lasers Surg Med 11.

[30] Hammer, M., A. Roggan, D. Schweitzer and G. Müller (1995) Optical properties of ocular fundus tissues – an in vitro study using the double-integrating-sphere technique and inverse Monte Carlo simulation, Phys Med Biol 40.

[31] Roider J. and Birngruber R. (1995) Solution of the heat conduction equation, In Optical-Thermal Response of Laser-Irradiated Tissue, Ed. A.J. Welch and van Gemert M.J.C., Plenum press, New York.

[32] Davis, T.P. and Mautner W.J. (1969) Helium-Neon laser effects on the eye, US Army Medical Research Laboratory, Annual report, Fort Detrick, Maryland.

[33] Frisch G.D., Beatrice E.S. and Holsen R.C. (1971) Comparative study of argon and ruby retinal damage thresholds, Invest Ophthal 10:11.

[34] Cain C.P., Toth C.A., Thomas R.J. et al. (2000) Comparison of macular versus paramacular retinal sensitivity to femtosecond laser pulses, J Biomed Opt 5:3.

[35] Weiter J.J., Delori F.C. et al. (1986) Retinal pigment epithelial lipofuscin and melanin and choroidal melanin in human eyes, Invest Ophthal Vis Sci 27.

[36] Spraul C.W., Lang G.E. and Grossniklaus H.E. (1996) Morphometric analysis of the choroid, Bruch's membrane and retinal pigment epithelium in eyes with age-related macular degeneration, Invest Ophthal Vis Sci 37:13.

[37] Snodderly D.M., Sandstrom M.M., Leung I.Y.-F. et al. (2002) Retinal pigment epithelial cell distribution in central retina of Rhesus monkeys. Invest Ophthal Vis Sci 43:9.

[38] Feeney-Burns L., Hilderbrand E.S. and Eldridge S. (1984) Aging human RPE: morphometric analysis of macular, equatorial and peripheral cells, Invest Ophthal Vis Sci 25:2.

[39] Gray D.C., Merigan W., Wolfing J.I. et al. (2006) In vivo fluorescence imaging of primate retinal ganglion cells and retinal pigment epithelial cells, Optics Express 14:16.

[40] Coogan P.S., Hughes W.F. and Molsen J.A. (1974) Histologic and spectrophotometric comparisons of the human and rhesus monkey retina and pigmented ocular fundus, USAF School of Aerospace Medicine, Final report, Brooks, Texas.

[41] Vogel A. and Birngruber R. (1992) Temperature profiles in human retina and choroid during laser coagulation with different wavelengths ranging from 514 to 810 nm, Laser Light Ophthal 5:1.

[42] Zagers N.P.A. and van Norren D. (2004) Absorption of the eye lens and macular pigment derived from the reflectance of cone photoreceptors, J Opt Soc Am A 21:12.

[43] Jacques S.L., Glickman R.D. and Schwartz J.A. (1996) Internal absorption coefficient and threshold for pulsed laser disruption of melanosomes isolated from retinal pigment epithelium, Ed. Jacques S.L., Proc. of SPIE vol. 2681.

[44] Prahl S., Optical absorption of hemoglobin, Webpage *omlc.ogi.edu/spectra/hemoglobin* (retrieved January 16th 2013)

[45] Berman E. R., Schwell H. and Feeney L. (1974) The retinal pigment epithelium: chemical composition and structure, Invest Ophthal 13:9.

[46] Neumann J. and Brinkmann R. (2005) Boiling nucleation on melanosomes and microbeads transiently heated by nanosecond and microsecond laser pulses, J Biomed Opt 10:2.

[47] Lepock J.R. (2003) Cellular effects of hyperthermia: relevance to the minimum dose for thermal damage, Int J Hyperthermia 19:3.

[48] Matylevitch N.P., Schuschereba S.T., Mata J.R. et al. (1998) Apoptosis and accidental cell death in cultured human keratinocytes after thermal injury, Am J Pathol 153:2.

[49] Schulmeister K., Seiser B., Edthofer F. et al. (2007) Retinal thermal damage threshold studies for multiple pulses, Proc. of SPIE vol. 6426.

[50] Jacques S.L. (2006) Ratio of entropy to enthalpy in thermal transitions in biological tissues, J Biomed Opt 11:4.

[51] Beatrice E.S. and Steinke C. (1972) Q-switched ruby retinal damage in Rhesus monkey, Joint AMRDC-AMC laser safety team, Report R-2051, Frankford Arsenal, Philadelphia.

[52] Borland R.G., Brennan D.H., Marshall J. and Viveash J.P. (1978) The role of fluorescein angiography in the detection of laser-induced damage to the retina, Exp Eye Res 27.

[53] Lund D.J., Stuck B.E. and Edsall P.R. (2006) Retinal injury thresholds for blue wavelength lasers, Health Phys 90:5.

[54] Gibbons W.D. (1974) Threshold damage evaluation of long-term exposures to argon laser radiation, USAF School of aerospace medicine, Report SAM-TR-74-29, Brooks, Texas.

[55] Lappin P.W. (1971) Assessment of ocular damage thresholds for laser radiation, Am J Optom 48:7.

[56] Gibbons W.D. and Allen R.G. (1975) Evaluation of retinal damage produced by long-term exposure to laser radiation, USAF School of aerospace medicine, Report SAM-TR-75-11, Brooks, Texas.

[57] Lund D.J., Edsall P.R., Stuck B.E. and Schulmeister K. (2007) Variation of laser-induced retinal injury thresholds with retinal irradiated area: 0.1-s duration, 514-nm exposures, J Biomed Opt 12:2.

[58] Lund D.J. (2009) New data on large spot threshold variation (private communication, unpublished)

[59] Roach W., Thomas R., Buffington G. et al. (2006) Simultaneous exposure using 532 and 860 nm lasers for visible lesion thresholds in the Rhesus retina, Health Phys 90:3.

[60] Vassiliadis A., Rosan R.C. and Zweng H.C. (1969) Research on ocular laser thresholds, USAF School of aerospace medicine, Final report, Brooks, Texas.

[61] Beatrice E.S. and Frisch G.D. (1973) Retinal laser damage thresholds as a function of image diameter, Arch Environ Health 27.

[62] Kirk E.C. (2001) Comparative morphology of the eye in primates, In The Anatomical record Part A, Wiley & Sons, ISSN 15524892.

[63] Kim C.B.Y., Ver Hoeve J.N., Kaufman P.L. and Nork T. (2004) Interspecies and gender differences in multifocal electroretinograms of cynomolgus and rhesus macaques, Doc Ophthal 109.

[64] Lund B.J., Lund D.J. and Edsall P.R. (2008) Laser-induced retinal damage threshold measurements with wavefront correction, J Biomed Opt 13:6.

[65] Vassiliadis A., Peppers N.A., Peabody R.R. et al. (1967) Investigations of laser damage to ocular tissues, Air Force Avionics Laboratory, Report AFAL-TR-67-170, Ohio.

[66] Vassiliadis A., Peppers N.A., Rosan R.C. et al. (1968) Investigations of laser damage to ocular tissues, USAF School of Aerospace Medicine, Final report, Brooks, Texas.

[67] Vassiliadis A., Zweng A.C. and Dedrick K.G. (1971) Ocular laser threshold investigations, USAF School of Aerospace Medicine, Final report, Brooks, Texas.

[68] Zuclich J.A., Lund D.J., Edsall P.R. et al. (2001) High-power lasers in the 1.3-1.4 μm wavelength range: ocular effects and safety standard implications, Proc. of SPIE, vol. 4246.

[69] Oliver J. W., Rockwell B.A., Kumru S.S. et al. (2011) Minimum visible lesion thresholds in Cynomolgus retina resulting from laser exposure at wavelengths of 413 nm, 532 nm and 647 nm, ILSC Conf. Proc. #803.

[70] Ham W.T., Mueller H., Ruffolo J.J. and Clarke A.M. (1979) Sensitivity of the retina to radiation damage as a function of wavelength, Photochem Photobiol 29:4.

[71] Bresnick G.H., Frisch G.D., Powell J.O. et al. (1970) Ocular effects of argon laser radiation; I. Retinal damage threshold studies, Invest Ophthal 9:11.

[72] Dunsky I.L. and Lappin P.W. (1971) Evaluation of retinal thresholds for c.w. laser radiation, Vis Res 11.

[73] Ham W.T., Mueller H., Ruffolo J.J. et al. (1984) Basic mechanisms underlying the production of photochemical lesions in the mammalian retina, Current Eye Research 3:1.

[74] Hemstreet H.W., Connolly J.S. and Egbert D.E. (1978) Ocular hazards of picosecond and repetitive-pulsed lasers Volume I, USAF School of Aerospace Medicine, Report SAM-TR-78-20, Brooks, Texas.

[75] L'Espérance F.A. and Kelly G.R. (1969) The threshold of the retina to damage by argon laser radiation, Arch Ophthal 81.

[76] Lund D.J. and Beatrice E.S. (1979) Ocular hazard of short pulse argon laser irradiation, Health Phys 36.

[77] Lund D.J., Stuck B.E. and Beatrice E.S. (1981) Biological research in support of project MILES, Letterman Army Institute of Research, Report #96, San Francisco.

[78] Lund D.J., Fuller D.R., Hoxie S.W. and Edsall P.R. (1997) Variation of retinal ED_{50} with exposure duration for near-IR sources, Proc. of SPIE vol. 2974.

[79] Sanders V.E. (1974) Wavelength dependence on threshold ocular damage from visible laser light Part I, USAF School of Aerospace Medicine, Annual report, Brooks, Texas.

[80] Skeen C.H., Bruce W.R., Tips J.H. et al. (1972) Ocular effects of near infrared laser radiation for safety criteria, USAF School of Aerospace Medicine, Final report, Brooks, Texas.

[81] Tata D.B., Stolarski D.J., Schuster K. et al. (2005) Photochemical and thermal retinal damage thresholds from an extended krypton laser source, ILSC Conf. Proc. #102.

[82] Vincelette R.L., Rockwell B.A., Oliver J.W. et al. (2009) Trends in retinal damage thresholds from 100-millisecond near-infrared laser radiation exposures, Laser Surg Med 41:5.

[83] Zuclich J.A., Griess G.A. et al. (1978) Research on the ocular effects of laser radiation, USAF School of Aerospace Medicine, Annual report, Brooks, Texas.

[84] Zuclich J.A. and Blankenstein M.F. (1988) Additivity of retinal damage for multiple-pulse laser , USAF School of Aerospace Medicine, Report SAM-TR-88-24, Brooks, Texas.

[85] Zuclich J.A., Zwick H., Schuscheraba S.T. et al. (1998) Ophthalmoscopic and pathologic description of ocular damage induced by infrared laser radiation, J Laser Appl 10:3.

[86] Polhamus G., Thomas R. and Hall R. (2002) Modeling of laser-induced threshold damage in the peripheral retina, Ed. Jacques S.L. et al., Proc. of SPIE vol. 4617.

[87] Navarro R., Artal P. and Williams D.R. (1993) Modulation transfer of the human eye as a function of retinal eccentricity, J Opt Soc Am A 10:2.

[88] Polhamus G.L. and Cohoon D.K. (unpublished) The spread function in the Rhesus, 22p.

[89] Sliney D.H. (2005) What is the minimal retinal image size? Implications for setting MPEs, ILSC Conf. Proc. #104.

[90] Wolbarsht M.L. (1999) The optics and physiology of the eye in relation to laser injury, ILSC Conf. Proc., p. 93-9.

[91] Welch A.J., Priebe L.A., Forster L.D. et al. (1979) Experimental validation of thermal retinal models of damage from laser radiation, USAF School of Aerospace Medicine, Report SAM-TR-79-9, Brooks, Texas.

[92] Schulmeister K., Husinsky J., Seiser B. et al. (2006) Ex-plant retinal laser induced threshold studies in the millisecond time regime, Proc. of SPIE vol. 6084.

[93] Lee H., Alt C., Pitsillides C.M. and Lin C.P. (2007) Optical detection of intracellular cavitation during selective laser targeting of the retinal pigment epithelium, J Biomed Opt 12:6.

[94] Herrmann K., Flöhr C., Stalljohann J. et al. (2007) Influence of choroidal perfusion on retinal temperature increase during retinal laser treatments, Proc. of SPIE vol. 6632.

[95] Lund B.J. (2006) Laser retinal thermal damage threshold: impact of small-scale ocular motion, J Biomed Opt 11:6.

[96] Dewhirst M.W., Viglianti B.L., Lora-Michiels M. et al. (2003) Basic principles of thermal dosimetry and thermal thresholds for tissue damage from hyperthermia, Int J Hyperthermia 19:3.

[97] Stuck B.E. (1984) Ocular susceptibility to laser radiation: human vs Rhesus monkey, Letterman Army Institute of Research, Handbook of laser bioeffects assessment volume 1, Chapter 4, San Francisco.

[98] Gabel V-.P., Birngruber R. and Hillenkamp F. (1978) Visible and near infrared in pigment epithelium and choroid, Ed. Shimuzu K. and Oosterhuis J.A., XXIII Concilium Ophthal, Kyoto.

[99] Ham W.T. and Müller H.A. (1989) The photopathology and nature of the blue light and near-UV retinal lesions produced by lasers and other optical sources, Ed. Wolbarsht M.L., In Laser Appl Med Biol, Chapter 5, Plenum Press.

[100] Marshall J., Hamiltion A.M. and Bird A.C. (1975) Histopathology of ruby and argon lesions in human and monkey retina, Brit J Ophthal 59.

Meet the authors

Mathieu Jean received his Master's degree in physical acoustics from the University Pierre & Marie Curie in Paris and is with the Seibersdorf Laboratories since 2007. He has developed physics-based models of thermally-induced damage to ocular tissues and skin, which he applies both to produce data to improve international exposure limits as well as for injury risk analysis of commercial products. Since 2008, he works on his PhD at the Univ. Techn. Vienna on laser induced injury modeling.

Karl Schulmeister, PhD, is a consultant on laser and broadband radiation safety at the Seibersdorf Laboratories, where also a specialized accredited test house is operated. Karl is a member of ICNIRP SCIV as well as of ANSI ASC Z136 TSC-1 (Bioeffects). He also serves as the secretary of IEC TC 76 WG1, the working group responsible for IEC 60825-1. The research in his group over the last eight years concentrated on thermally induced injury that also provided the basis for amending the spot size dependence and pulse additivity rules of the retinal thermal exposure limits in ICNIRP, ANSI and IEC laser safety guidelines.